

Crust-core interface and bulk neutron star properties

Ch. Margaritis,* P.S. Koliogiannis,† and Ch.C. Moustakidis‡

Department of Theoretical Physics, Aristotle University of Thessaloniki, 54124 Thessaloniki, Greece

The nuclear symmetry energy plays an important role in the description of the properties of finite nuclei as well as neutron stars. Especially, for low values of baryon density, the accurate description of the crust-core interface strongly depends on the symmetry energy. Usually, the well known parabolic approximation is employed for the definition of the symmetry energy without avoiding some drawbacks. In the present work, a class of nuclear models, suitable for the description of the inner and outer core of neutron stars, is applied in studying the effect of higher orders of the expansion of the energy on the location of the crust-core transition. The thermodynamical and dynamical methods are used for the determination of the transition density n_t and pressure P_t . The corresponding energy density functional is applied for the study of some relevant properties of both non-rotating and slow rotating neutron stars. We found that the larger the value of the slope parameter L , the slower the convergence of the expansion. In addition, a universal relation is presented between n_t and L , by employing the full expression and dynamical approach. The crustal moment of inertia is very sensitive on the location of the transition while the effects are moderated concerning the critical angular velocity of the r-mode instability and minimum mass configuration. The effect on the tidal deformability is less but not negligible. In any case, the use of the parabolic approximation leads to the overestimation of n_t and P_t and consequently, on inaccurate predictions.

PACS numbers: 26.60.+c, 97.60.Jd, 21.65.+f

Keywords: Equation of state; Symmetry energy; Neutron star

I. INTRODUCTION

The equation of state (EoS) of neutron-rich nuclear matter is the main ingredient in the study of the structure and properties of neutron stars [1–5]. Moreover, the observations of neutron stars provide useful constraints concerning the EoS both for low and high nuclear matter densities. In particular, of great interest are the properties related to the interface between the crust and core, including mainly the transition density and the corresponding transition pressure. These quantities are sensitive on the behavior of the EoS at low densities and play important role on the predictions of some bulk neutron star properties. To be more specific, the inner crust comprises the outer region from the density at which neutrons drip out of nuclei to the inner edge, separating the solid crust from the homogeneous liquid core. At the inner edge a phase transition occurs from the high density homogeneous matter to the in-homogeneous one at lower densities. It was found that the transition density determines the structure of the inner part of the neutron star’s crust and also is related to some finite nuclei properties including neutron-skin, dipole polarizability, etc. [6–8].

The determination of the transition density n_t itself is a very complicated problem because the inner crust may have an intricate structure. A well established approach is to find the density at which the uniform liquid becomes unstable with respect to small-amplitude density fluctuations, indicating the formation of nuclear clusters.

This approach includes mainly the dynamical method [9–18], the thermodynamical one [19–23], the random phase approximation [8, 24], and the Vlasov method [25, 26]. Recently, in a notable work, Carreau *et al.* [27] studied the crust-core transition within a unified meta-modeling of the nuclear EoS where the variational equations in the crust are solved within a Compressible Liquid-Drop (CLD) approach.

The motivation of the present work is twofold. Firstly, we intend to study more systematically the convergence of the baryon energy per particle expansion around the asymmetry parameter $I = (n_n - n_p)/(n_n + n_p)$, where n_n and n_p are the neutron and proton number densities, respectively. It is well known that keeping only a quadratic term of I , the accuracy of the expansion is sufficient. Most of the relevant studies use this order of the expansion, which is well known as the parabolic approximation. In recent studies, the effects of additional terms have been considered, usually up to order of $\mathcal{O}(I^6)$ [18]. In the present work we extend the study up to the order of $\mathcal{O}(I^{10})$, conjecturing that it is sufficient to gain the main conclusion about the speed of convergence of the expansion. In particular, we employ the energies per baryon, originated by various nuclear models, mainly focus on the role played by the slope of the symmetry energy L at the saturation density and its effect on the growth of the convergence speed. Moreover, we employed both the dynamical and thermodynamical method to calculate the transition density and pressure, corresponding to the crust-core interface for each expansion term. We mainly focus on the parabolic approximation (PA) and the full expression (FE) (which includes all terms).

Secondly, we apply our findings in order to examine the effect of the two cases on some neutron star properties

* chmargar@auth.gr

† pkoliogi@physics.auth.gr

‡ moustaki@auth.gr

that we expect to be sensitive on the values of n_t and P_t . To be more specific, we concentrate on the crustal moment of inertia both of non-rotating and slowly rotating neutron stars, the critical frequency of the r-mode instability, the tidal deformability, and the minimum mass configuration. Finally, we analyze and discuss the extent of the effects of the crust-core interface on each of the latter properties.

The article is organized as follows: In Sec. II we present the energy expansion, the symmetry energy and the corresponding slope parameter. In Sec. III we briefly summarize the dynamical and the thermodynamical method for the determination of the transition density and pressure, while in Sec. IV we present the specific neutron star properties related to the crust-core interface. In Sec. V we present the results of the present study and discuss their implications. Finally, Sec. VI includes the concluding remarks.

II. SYMMETRY ENERGY

The energy per baryon $E_b(n, I)$ of asymmetric nuclear matter can be expanded around the asymmetry parameter I as [22, 28]

$$E_b(n, I) = E_b(n, I = 0) + \sum_{k=1} E_{\text{sym},2k}(n) I^{2k}. \quad (1)$$

The asymmetry parameter can be written as $I = 1 - 2x$, where x is the proton fraction n_p/n . Moreover, in Eq. (1), $E_b(n, I = 0)$ denotes the energy per baryon of the symmetric nuclear matter. The coefficients of the expansion in Eq. (1) are given by the expression

$$E_{\text{sym},2k}(n) = \frac{1}{(2k)!} \left. \frac{\partial^{2k} E_b(n, I)}{\partial I^{2k}} \right|_{I=0}. \quad (2)$$

Since the strong interaction must be symmetric under the exchange of neutrons with protons, only even powers of I appear in Eq. (1). The nuclear symmetry energy is, by definition, the coefficient of the quadratic term $E_{\text{sym},2}(n)$. The slope parameter L is an indicator of the stiffness of the EoS and is defined as

$$L = 3n_s \left. \frac{dE_{\text{sym},2}(n)}{dn} \right|_{n=n_s}, \quad (3)$$

where n_s is the nuclear saturation density.

We can define also the slope parameter L_{2k} , which corresponds to higher order terms, using Eq. (2) (see also Ref. [18]), according to the rule

$$L_{2k} = 3n_s \left. \frac{dE_{\text{sym},2k}(n)}{dn} \right|_{n=n_s}. \quad (4)$$

Keeping in Eq. (1) terms only up to a quadratic one, and defining the symmetry energy as the difference between the energy per baryon in pure neutron matter and

symmetric nuclear matter, we lead to the parabolic approximation of the symmetry energy according to the law

$$E_{\text{sym}}^{\text{PA}}(n) = E_b(n, I = 1) - E_b(n, I = 0). \quad (5)$$

The slope parameter L_{PA} , that corresponds to the parabolic approximation, is found by Eq. (3) by replacing $E_{\text{sym},2}(n)$ with $E_{\text{sym}}^{\text{PA}}(n)$. It is worth to mention here that in general, the definitions of $E_{\text{sym},2}(n)$ and $E_{\text{sym}}^{\text{PA}}(n)$ do not coincide. This is the case only when the energy per baryon includes terms up to a quadratic one of the asymmetry parameter I .

III. DYNAMICAL AND THERMODYNAMICAL METHOD

The crust-core interface is related to the phase transition between nuclei and uniform nuclear matter. The latter one is nearly pure neutron matter, as the proton fraction is just a few percent, determined by the condition of β -equilibrium. The study of the instability of β -stable nuclear matter is based on the variation of the total energy density, in the framework of the Thomas-Fermi approximations [9, 10]. In the dynamical method, compared to the thermodynamical one, effects due to inhomogeneity of the density and the Coulomb interaction have also been included. The onset of instability will occur if the total energy, in the presence of the density inhomogeneity, is lower than the energy of the uniform phase. The key expression for the description of the instability reads [9, 10, 17] as

$$U_{\text{dyn}}(n) = U_0(n) + 4\sqrt{\pi\alpha\hbar c\xi} - 4\alpha\xi (9\pi x^2 n^2)^{1/3}, \quad (6)$$

where $\alpha = e^2/\hbar c$,

$$U_0(n) = \frac{\partial\mu_p}{\partial n_p} - \frac{(\partial\mu_p/\partial n_n)^2}{\partial\mu_n/\partial n_n}, \quad (7)$$

and

$$\xi = 2D_{nn}(1 + 4\zeta + \zeta^2), \quad \zeta = -\frac{\partial\mu_p/\partial n_n}{\partial\mu_n/\partial n_n}. \quad (8)$$

The chemical potentials μ_n and μ_p are defined as

$$\mu_n = \left(\frac{\partial E_b}{\partial n_n} \right)_{n_p}, \quad \mu_p = \left(\frac{\partial E_b}{\partial n_p} \right)_{n_n}. \quad (9)$$

The transition density n_t is determined from the condition $U_{\text{dyn}}(n_t) = 0$.

The key expression of the thermodynamical method is the following (for more details see Refs. [19–22])

$$C_{\text{therm}}(n) = 2n \frac{\partial E(n, x)}{\partial n} + n^2 \frac{\partial^2 E(n, x)}{\partial n^2} - \left(\frac{\partial^2 E(n, x)}{\partial n \partial x} n \right)^2 \left(\frac{\partial^2 E(n, x)}{\partial x^2} \right)^{-1}, \quad (10)$$

and the transition density n_t is now determined from the condition $C_{\text{therm}}(n_t) = 0$.

In both cases, the proton fraction x , is determined as a function of the baryon density n from the condition of β -equilibrium. In particular, in β -stable nuclear matter, the chemical equilibrium condition takes the form

$$\mu_n = \mu_p + \mu_e. \quad (11)$$

It is easy to show that after some algebra we get [17, 22]

$$\mu_n - \mu_p = \left(-\frac{\partial E_b}{\partial x} \right)_n. \quad (12)$$

Now, since the electron chemical potential μ_e is given by

$$\mu_e = \hbar c (3\pi^2 n_e)^{1/3}, \quad (13)$$

we finally found

$$\left(\frac{\partial E_b}{\partial x} \right)_n = -\hbar c (3\pi^2 x n)^{1/3}. \quad (14)$$

Eq. (14) is solved numerically and an expression for x as a function of n is found.

Another important quantity is the transition pressure P_t . Both baryons and leptons contribute to the total pressure, meaning that the transition pressure is given by the following relation [21, 22]

$$P_t^{\text{FE}}(n_t, x_t) = n_t^2 \frac{\partial E_b}{\partial n} \Big|_{n=n_t} + \frac{\hbar c}{12\pi^2} (3\pi^2 x_t n_t)^{4/3}, \quad (15)$$

where x_t is the proton fraction related to the transition density.

IV. APPLICATION ON NEUTRON STAR PROPERTIES

The EoS of nuclear matter is the key ingredient to study the bulk properties of neutron stars. However, there are some specific ones which depend directly on the location of the crust-core interface. This class of properties includes the fraction of moment of inertia of the crust with respect to the total one, the critical angular frequency which defines the r-mode instability, the tidal polarizability, and the minimum mass configuration. To be more specific, the crustal moment of inertia I_{crust}/I and the critical angular velocity Ω_c , by definition depend on the crust-core interface. On the other hand, tidal deformability λ of a low mass neutron star is sensitive on the specific details of the crust [29–32], while minimum mass configuration mainly depends on the contribution of the crust both to M_{min} and R_{min} . In the latter, since the central density is close to the transition density, it is expected that even a slight shift to n_t (and P_t) will modify the relevant predictions.

A. Crustal fraction of the moment of inertia

The crustal moment of inertia plays an important role on the evolution of neutron stars and the exhibition of some specific phenomena. It is particularly interesting since it can be inferred from observations of pulsar glitches, the occasional disruptions of the otherwise extremely regular pulsations of magnetized, rotating neutron stars. In the case of a non-rotating (or slow rotating) neutron star a few elaborated approximations have been performed leading to analytical predictions of I_{crust} . These approximations depend directly on the transition pressure P_t (or/and the transition density n_t). The most used one was provided in Ref. [33] and is written as

$$\frac{I_{\text{crust}}}{I} \simeq \frac{28\pi P_t R^3}{3Mc^2} \frac{(1 - 1.67\beta - 0.6\beta^2)}{\beta} \times \left(1 + \frac{2P_t}{n_t mc^2} \frac{(1 + 5\beta - 14\beta^2)}{\beta^2} \right)^{-1}, \quad (16)$$

where $\beta = GM/Rc^2$ is the compactness parameter.

We also apply for comparison a second approximation [34] given by

$$I_{\text{crust}} \simeq \frac{16\pi}{3} \frac{R_{\text{core}}^6}{2\beta c^2 R} P_t \left(1 - \frac{0.21}{1 - 2\beta} 2\beta \right) \times \left[1 + \frac{48}{5} \left(\frac{R_{\text{core}}}{2\beta R} - 1 \right) \left(\frac{P_t}{\mathcal{E}_t} \right) + \dots \right]. \quad (17)$$

In general, the moment of inertia of rotating neutron stars exhibits dependence on the spin frequency [35] and in this case, the calculation of the crustal moment of inertia demands special treatment. However, it is worth noticing that approximations (16) and (17) are sufficiently accurate also for a slow rotating neutron star, that is rotating with angular velocity $\Omega \ll \Omega_k$, where Ω_k is the Kepler angular velocity [34].

B. Critical angular velocity for r-modes

The *r*-modes are oscillations of rotating stars whose restoring force is the Coriolis force (see Refs. [36–38] and references therein). The gravitational radiation-driven instability of these models has been proposed as an explanation for the observed relatively low spin frequencies of young neutron stars and of accreting ones in low-mass x-ray binaries (LMXBs). This instability can only occur when the gravitational-radiation driving time scale of the *r*-mode is shorter than the time scales of the various dissipation mechanisms that may occur in the interior of the neutron star. The instability condition reads as [36–39]

$$\frac{1}{\tau_{\text{GW}}} + \frac{1}{\tau_{ee}} + \frac{1}{\tau_{nn}} = 0, \quad (18)$$

where τ_{ee} and τ_{nn} are the time scales of the various dissipation mechanisms (due to electron-electron and neutron-neutron scattering respectively) which are considered in

the present study. The condition (18) leads to the critical angular velocity Ω_c which is given by (for a detailed analysis see Refs. [17, 39, 40])

$$\frac{\Omega_c}{\Omega_0} = \left(-\frac{\tilde{\tau}_{\text{GW}}(\tilde{\tau}_{ee} + \tilde{\tau}_{nn})}{\tilde{\tau}_{ee}\tilde{\tau}_{nn}} \right)^{2/11} \left(\frac{10^8 \text{K}}{T} \right)^{2/11}, \quad (19)$$

where $\Omega_0 = \sqrt{3GM/4R^3}$, T is the temperature, and also

$$\tau_{\text{GW}} = \tilde{\tau}_{\text{GW}} \left(\frac{\Omega_0}{\Omega} \right)^6, \quad \tau_{ii} = \tilde{\tau}_{ii} \left(\frac{\Omega_0}{\Omega} \right)^{1/2} \left(\frac{10^8 \text{K}}{T} \right),$$

with $ii = ee, nn$. In the present work we will concentrate in the case where the main damping mechanism is due to the viscous dissipation at the boundary layer of the perfectly rigid crust and fluid core. In this case, the corresponding critical angular velocity takes the form [17, 39])

$$\Omega_c = 1.93795 \times 10^5 \left(\frac{R_{\text{core}}}{\text{km}} \right)^{12/11} \left(\frac{\mathcal{E}_t}{\text{MeV fm}^{-3}} \right)^{3/11} \times \left(1 + 0.25865 \left(\frac{\mathcal{E}_t}{\text{MeV fm}^{-3}} \right)^{1/8} \right)^{2/11} \times I(R_{\text{core}})^{-4/11} \left(\frac{10^8 \text{K}}{T} \right)^{2/11}. \quad (20)$$

From Eq. (20) is obvious the direct dependence of Ω_c on the crust-core interface via \mathcal{E}_t , as well as the indirect one via the values of the core radius R_{core} and the integral $I(R_{\text{core}})$ where

$$I(R_{\text{core}}) = \int_0^{R_{\text{core}}} \left(\frac{\mathcal{E}(r)}{\text{MeV fm}^{-3}} \right) \left(\frac{r}{\text{km}} \right)^6 d \left(\frac{r}{\text{km}} \right), \quad (21)$$

with $\mathcal{E}(r)$ being the energy density of neutron star matter at distance r from the center.

C. Tidal deformability

Gravitational waves from the final stages of inspiraling binary neutron stars are one of the most important sources for ground-based gravitational wave detectors [41, 42]. Flanagan and Hinderer [43] have pointed out that tidal effects are also potentially measurable during the early part of the evolution when the waveform is relatively clean. The tidal fields induce quadrupole moments on the neutron stars. The response of the neutron star is described by the dimensionless so-called Love number k_2 which depends on the structure of the neutron star (both core and crust). The Love number is linearly related to the tidal deformability λ according to $\lambda = 2R^5 k_2 / 3G$.

Now, k_2 is given by [44]

$$k_2 = \frac{8\beta^5}{5} (1 - 2\beta)^2 [2 - y_R + (y_R - 1)2\beta] \times \left[2\beta (6 - 3y_R + 3\beta(5y_R - 8)) + 4\beta^3 (13 - 11y_R + \beta(3y_R - 2) + 2\beta^2(1 + y_R)) + 3(1 - 2\beta)^2 [2 - y_R + 2\beta(y_R - 1)] \ln(1 - 2\beta) \right]^{-1} \quad (22)$$

where the quantity $y_R \equiv y(R)$ is determined by solving the relevant differential equation of $y(r)$ simultaneously with the Tolman-Oppenheimer-Volkoff equations [44]. It is noted that the measure of the amplitude of the radiated gravitational waves provides information for the tidal deformability and consequently useful constraints on bulk neutron stars properties, including mainly the radius. We expect that due to the strong dependence of λ on R and also on the Love number k_2 , the effects of the crust-core interface may affect its value. In any case, this possibility is of interest and also worth to be under consideration.

D. Minimum mass configuration

The minimum neutron star mass, apart for the maximum one, is also of great interest in Astrophysics [45, 46]. Its knowledge is related to the case of a neutron star in a close binary system with a more compact partner (neutron star or black hole). In particular, the lower mass neutron star transfers mass to the more massive object, a process which ultimately leads to approaching its minimum value. Finally, crossing this value, the neutron star reaches a non equilibrium configuration. The minimum mass is a universal feature, independent of the details of the EoS and well constrained to the value $M_{\min} \simeq 0.1 M_{\odot}$. This is because the corresponding central densities are close to the values of the transition densities n_t . Now, since the equation of the crust is well known, all theoretical predictions for M_{\min} converge. However, the corresponding radius R_{\min} is very sensitive on the details of the EoS. We expect that the location of the crust-core transition will affect appreciably the values of R_{\min} . In the present study we investigate in which extent R_{\min} is affected by the values of n_t (and P_t).

V. RESULTS AND DISCUSSION

In the present work, we compare a class of EoSs generated from three different nuclear models. In particular, we employ a momentum dependent interaction model (MDI) which was presented and analyzed in previous papers [47, 48]. The parametrization of the model has been chosen in order to generate specific values for $E_{\text{sym},2}(n_s)$ and the slope parameter L at the saturation density n_s . The second one (HLPS), is based on the microscopic

TABLE I. Transition density (in units of fm^{-3}) and pressure (in units of MeV fm^{-3}) calculated using the full expression for each nuclear model ($n_t^{\text{FE}}, P_t^{\text{FE}}$), the parabolic approximation ($n_t^{\text{PA}}, P_t^{\text{PA}}$) and approximations of each EoS based on Eq. (1) up to order $2k$ ($n_{t,2k}, P_{t,2k}$). All calculations are performed in the framework of the thermodynamical method.

Nuclear model	n_t^{FE}	P_t^{FE}	n_t^{PA}	P_t^{PA}	$n_{t,2}$	$P_{t,2}$	$n_{t,4}$	$P_{t,4}$	$n_{t,6}$	$P_{t,6}$	$n_{t,8}$	$P_{t,8}$	$n_{t,10}$	$P_{t,10}$
MDI(65)	0.078	0.317	0.097	0.594	0.094	0.641	0.092	0.519	0.090	0.477	0.088	0.449	0.086	0.428
MDI(72.5)	0.073	0.315	0.094	0.728	0.094	0.697	0.090	0.618	0.087	0.561	0.085	0.519	0.083	0.488
MDI(80)	0.068	0.286	0.094	0.836	0.095	0.783	0.090	0.684	0.086	0.608	0.084	0.553	0.082	0.513
MDI(95-30)	0.058	0.146	0.099	1.078	0.099	1.071	0.093	0.845	0.087	0.697	0.083	0.601	0.081	0.532
MDI(95-32)	0.064	0.277	0.097	1.054	0.097	1.026	0.091	0.857	0.087	0.742	0.084	0.662	0.081	0.604
MDI(100)	0.053	0.088	0.102	1.202	0.103	1.247	0.096	0.967	0.089	0.765	0.085	0.641	0.081	0.554
MDI(110)	0.047	0.047	0.106	1.484	0.109	1.723	0.108	1.548	0.094	0.993	0.088	0.799	0.083	0.658
HLPS(49.4)	0.089	0.551	0.097	0.694	0.098	0.675	0.095	0.651	0.094	0.630	0.093	0.614	0.092	0.602
HLPS(29.5)	0.098	0.455	0.104	0.495	0.105	0.513	0.103	0.509	0.102	0.500	0.101	0.492	0.100	0.485
Ski4(60.4)	0.081	0.337	0.091	0.496	0.091	0.481	0.089	0.453	0.087	0.432	0.086	0.416	0.085	0.404
Ska(76.1)	0.079	0.528	0.093	0.866	0.094	0.809	0.090	0.762	0.088	0.713	0.086	0.677	0.085	0.649
Sly4(46)	0.088	0.463	0.094	0.546	0.094	0.528	0.093	0.517	0.092	0.506	0.091	0.497	0.090	0.491

TABLE II. Transition density (in units of fm^{-3}) and pressure (in units of MeV fm^{-3}) calculated using the full expression for each nuclear model ($n_t^{\text{FE}}, P_t^{\text{FE}}$), the parabolic approximation ($n_t^{\text{PA}}, P_t^{\text{PA}}$) and approximations of each EoS based on Eq. (1) up to order $2k$ ($n_{t,2k}, P_{t,2k}$). All calculations are performed in the framework of the dynamical method.

Nuclear model	n_t^{FE}	P_t^{FE}	n_t^{PA}	P_t^{PA}	$n_{t,2}$	$P_{t,2}$	$n_{t,4}$	$P_{t,4}$	$n_{t,6}$	$P_{t,6}$	$n_{t,8}$	$P_{t,8}$	$n_{t,10}$	$P_{t,10}$
MDI(65)	0.070	0.232	0.086	0.425	0.084	0.488	0.082	0.365	0.080	0.339	0.077	0.322	0.077	0.309
MDI(72.5)	0.064	0.212	0.082	0.483	0.083	0.458	0.079	0.413	0.077	0.380	0.075	0.354	0.074	0.334
MDI(80)	0.060	0.181	0.082	0.529	0.082	0.492	0.078	0.441	0.076	0.396	0.074	0.363	0.072	0.337
MDI(95-30)	0.050	0.075	0.084	0.615	0.084	0.602	0.079	0.479	0.075	0.400	0.072	0.347	0.069	0.309
MDI(95-32)	0.055	0.157	0.082	0.641	0.083	0.618	0.078	0.524	0.075	0.457	0.072	0.409	0.070	0.374
MDI(100)	0.047	0.039	0.085	0.656	0.086	0.670	0.079	0.508	0.075	0.408	0.072	0.343	0.069	0.298
MDI(110)	0.042	0.016	0.088	0.804	0.090	0.919	0.085	0.699	0.077	0.488	0.072	0.392	0.069	0.325
HLPS(49.4)	0.079	0.415	0.087	0.525	0.087	0.509	0.085	0.493	0.084	0.478	0.083	0.466	0.082	0.457
HLPS(29.5)	0.091	0.339	0.093	0.366	0.094	0.403	0.093	0.376	0.092	0.376	0.091	0.371	0.090	0.399
Ski4(60.4)	0.073	0.248	0.082	0.356	0.082	0.343	0.080	0.327	0.079	0.314	0.078	0.304	0.077	0.296
Ska(76.1)	0.069	0.377	0.082	0.622	0.083	0.580	0.080	0.553	0.078	0.520	0.077	0.494	0.075	0.474
Sly4(46)	0.080	0.365	0.085	0.427	0.085	0.411	0.083	0.405	0.083	0.398	0.082	0.392	0.082	0.387

calculations, in the framework of chiral effective field theory interactions, in low densities and suitable polytropic parametrization at high nuclear densities [49]. Specifically, we employ two parametrizations of the model, the soft ($L = 29.5$ MeV) and the stiff ($L = 49.4$ MeV) ones (for more details see Ref. [49]). Lastly, we use three versions of the Skyrme model that is the Ski4, Ska and Sly4 [50, 51]. The above nuclear models are used to construct the EoS of the core of a neutron star. The EoS of the crust is taken from the well known model of Baym, Pethick, and Sutherland [52] (hereafter BPS model). Although, in the present study we mainly focus on the crust-core transition effects, the models have been chosen in order to produce, even marginally, the limit of the two solar masses.

In Tables I and II we present our calculations for the transition densities and the corresponding pressures. Inside the parenthesis is the value of the slope parameter L . Also, the specific cases MDI(95-30) and MDI(95-32) correspond to $L = 95$ MeV and $E_{\text{sym},2}(n_s) = 30$ MeV and $E_{\text{sym},2}(n_s) = 32$ MeV, respectively. The calculations are performed using both the thermodynamical and the dynamical method. In each case, we employed the full

expression of the energy per baryon of each model, the parabolic approximation (see Eq. (5)) and the corresponding terms of the expansion (see Eq. (1)) up to tenth order. In order to clarify further the predictions, we display the results also in Fig. 1.

In each case, the higher the order in the expansion, the lower the values of n_t and P_t . Even more, the higher the value of the slope parameter L , the larger the deviation between the second order predictions and the consideration of the full expression. In other words, according to our finding, the lower the value of L , the higher the accuracy of the parabolic approximation. It is worth to mention here that the quadratic dependence of P_t on n_t (see Eq. (15)) is well reflected on the current predictions and mainly on the dispersion of the results for high values of L . As a general rule, the thermodynamical method leads to higher values of P_t on n_t compared to the dynamical one. However, the most distinctive feature is the appearing of a universal dependence of n_t on L in both methods concerning the full expression. We found that, independently of the employed model, there is an ordering on the mentioned dependence, where the increase of L ,

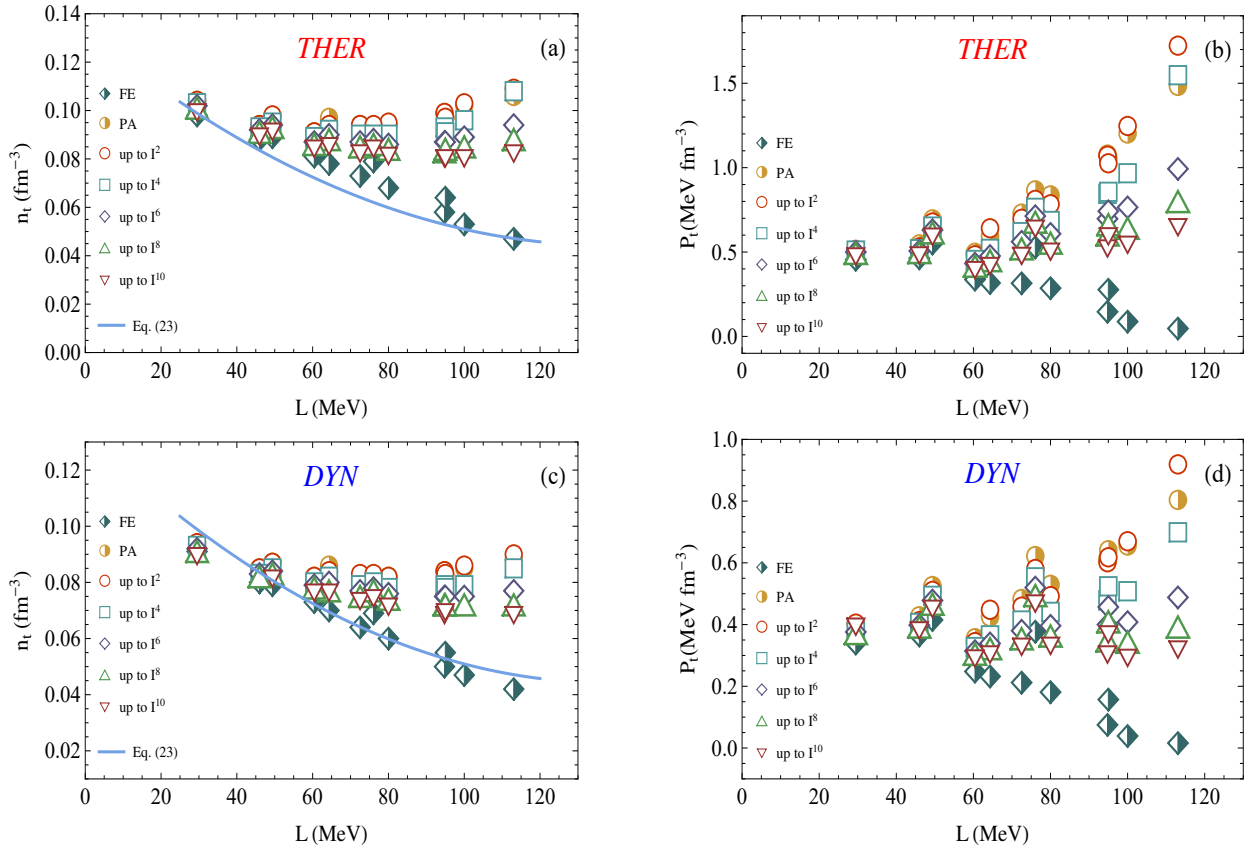


FIG. 1. Transition density n_t and pressure P_t as a function of the slope parameter L for various nuclear models. The calculations are performed with the thermodynamical method for (a,b) and the dynamical one for (c,d). The half-filled diamonds present the full expression, the half-filled circles present the parabolic approximation, and the circles, the squares, the diamonds, the triangles, and the reversed triangles present the approximation up to second, fourth, sixth, eighth, and tenth order, respectively, based on Eq. (1). The solid line in (a,c) represents the Eq. (23).

leads to a decreased n_t . In order to check our finding, we utilize the following expression, predicted by Steiner *et al.* [53]

$$n_t = S_{30} (0.1327 - 0.0898L_{70} + 0.0228L_{70}^2) \text{ (fm}^{-3}\text{)}, \quad (23)$$

where $S_{30} = E_{\text{sym},2}(n_s)/(30 \text{ MeV})$ and $L_{70} = L/(70 \text{ MeV})$. We found that there is an excellent agreement with the present results (see Fig. 1(a,c)), concerning the dynamical method, for a large interval of L and mainly for different nuclear models.

Moreover, we studied the effects of the crust-core interface on four specific properties of neutron stars. We employed in each case, as an example, the MDI(80) model. It has to be noted here that we found similar results for the rest of the models (depending of course on the value of the slope parameter L).

Crustal fraction: The effects of the symmetry energy on the crustal fraction of a non-rotating and slow rotating with $M = 1.4 M_\odot$ neutron star, are displayed in Fig. 2. In particular, we employed the approximations (16) and (17) for comparison. Our finding confirms previous predictions for a non-rotating neutron star, that is the crustal

moment of inertia is very sensitive on the location of the crust-core interface. In particular, in Fig. 2(a), we display the dependence of the crustal ratio I_{crust}/I on the mass. The application of the dynamical method, using the full expression, leads to the lower values of I_{crust}/I , compared to the thermodynamical one. The two horizontal lines represent, each one, a possible constraint on I_{crust}/I deduced for the Vela pulsar (assuming a neutron star with $M = 1.4 M_\odot$). The lower limit, 0.014, was suggested in Ref. [54], while the higher one, 0.07, was considered in Refs. [55, 56] in order to explain the glitches. It is notable, in Fig. 2(b), that the predictions of the approximations (16) and (17) are almost identical in the case of the full expression (in both methods), while distinct deviations appear in the case of the parabolic approximation. We conjecture that in the case of a rapidly rotating neutron star (close to the mass-shedding limit, that is the Kepler angular velocity) the effects of the symmetry energy expansion on I_{crust}/I will be dramatic. In this case, one must carefully select the appropriate method with the full expression. Otherwise, the accuracy of the predictions will suffer from large uncertainties.

r-mode instability: In the present study we concen-

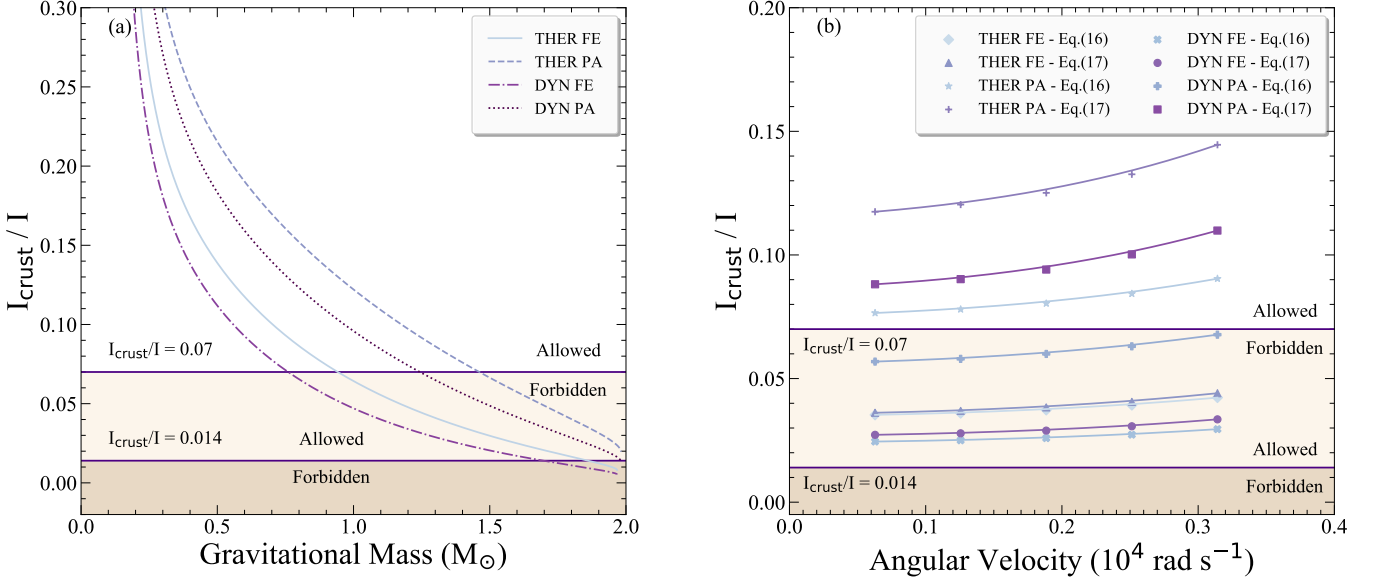


FIG. 2. (a) Crustal fraction of moment of inertia as a function of gravitational mass for the four selected cases using the approximation (16). (b) Crustal fraction of moment of inertia for a neutron star with $M = 1.4 M_{\odot}$ as a function of angular velocity for the four selected cases, using the approximations (16) and (17). The regions defined by the $I_{\text{crust}}/I = 0.07$ and $I_{\text{crust}}/I = 0.014$, which represent a possible constraint deduced for the Vela pulsar assuming a neutron star with $M = 1.4 M_{\odot}$, are also included (for more details see text).

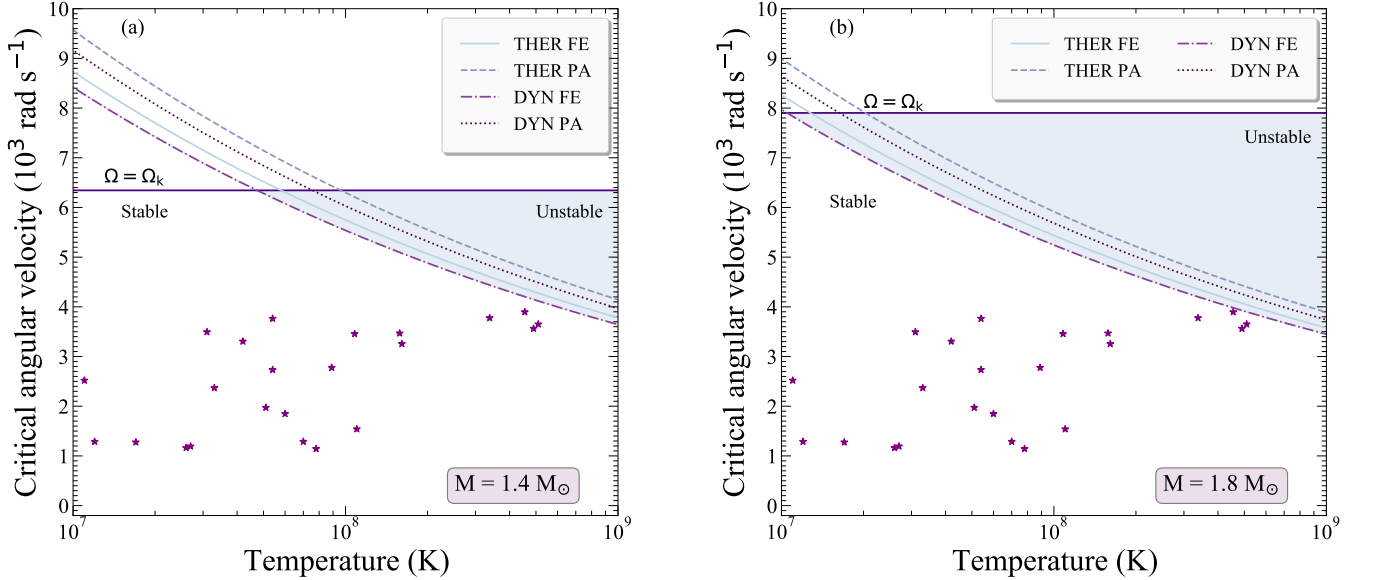


FIG. 3. Critical angular velocity as a function of temperature for the four selected cases for a neutron star with (a) $M = 1.4 M_{\odot}$ and (b) $M = 1.8 M_{\odot}$. For comparison, the observed cases of LMXBs and MSRPs from Haskell *et al.* [57] presented with stars and the horizontal lines, which correspond to the Kepler angular velocity Ω_k [35], are also included. The shaded region corresponds to the r-mode instability window.

trated also on the effects of the crust-core transition on the r-mode instabilities. According to Eq. (20), the critical angular velocity Ω_c is sensitive on the neutron star core radius R_{core} and energy density \mathcal{E}_t . In Fig. 3 we display the r-mode instability windows for the selected four cases (MDI model with $L = 80 \text{ MeV}$) and for $M = 1.4 M_{\odot}$ and

$M = 1.8 M_{\odot}$, respectively. Moreover, we included many cases of LMXBs and a few MSRPs (millisecond radio pulsars). It is worth to mention that the estimates of core temperature T have large uncertainties (see Ref. [57]). However, since the purpose of the present study is to exhibit the role of crust-core transition, more details on

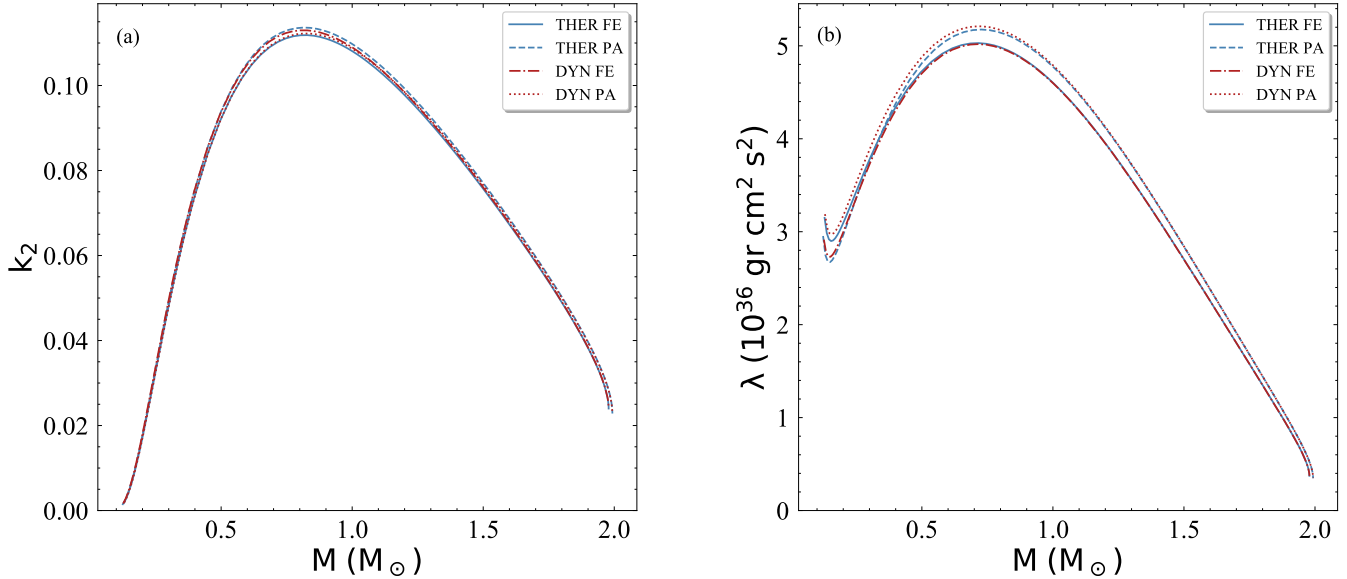


FIG. 4. (a) The tidal Love number k_2 and (b) the tidal deformability λ as a function of the gravitational mass for the four selected cases.

TABLE III. The minimum mass configuration (including the minimum mass M_{\min} , the corresponding radius R_{\min} , and central density ρ_c) of cold and non-rotating neutron stars using the MDI(80) nuclear model for the core and the BPS model [9] for the crust.

Nuclear model	$M_{\min} (M_\odot)$	$R_{\min} (\text{km})$	$\rho_c (10^{14} \text{ gr cm}^{-3})$
THER FE	0.0920	245	2.135
THER PA	0.0919	219	2.141
DYN FE	0.0896	255	2.154
DYN PA	0.0922	243	2.109

the temperature uncertainties are not included. The full expression cases (dynamical and thermodynamical) lead to lower values compared to the corresponding parabolic approximations, increasing the instability window. In other words, the parabolic approximation gives rise to a narrower instability window, for the same value of temperature. Therefore, since the damping due to viscous dissipation at the boundary layer of the perfectly rigid crust and fluid core is of major importance in r-mode studies, one has to use carefully the employed method for the estimation of the crust-core edge.

Tidal deformability: In Fig. 4 we display the Love number k_2 as a function of the mass for the four cases. Obviously, k_2 is almost insensitive on the approach. However, in the case of the tidal deformability λ , the effects are more pronounced especially for low neutron star mass. In particular, in the case of the full expression, both approaches lead to similar predictions while in the parabolic approximation, both cases lead to higher values of λ . In conclusion, the effects are small but not negligible.

Minimum mass of neutron star: In Fig. 5 we display

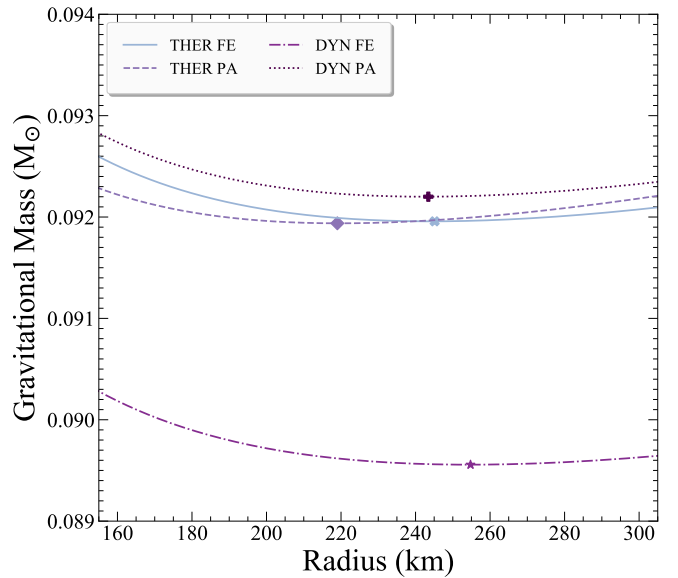


FIG. 5. Gravitational mass as a function of the radius near the minimum gravitational mass region, for the selected cases. Minimum mass configuration is indicated with a cross for the full expression and thermodynamical method, a diamond for the parabolic approximation and thermodynamical method, a star for the full expression and dynamical method, and a plus for the parabolic approximation and dynamical method.

the gravitational mass as a function of the radius near the minimum gravitational mass region. In addition, in Table III we present the minimum mass, the corresponding radius and central energy density for the four cases. It should be emphasized that an accurate treatment of

the minimum mass demands the use of the same nuclear model both for the core and the crust region (and consequently on the crust-core interface). However, since our main purpose was to examine the effect of the symmetry energy on the location of the transition density and pressure, we used the same nuclear model for the core while the EoS of the crust is taken from the well known BPS model [52].

Our predictions are close to those found by Haensel *et al.* [45] using two different nuclear models. Obviously, as expected, the effects on the minimum mass are almost negligible. However, the effects are more pronounced in the case of the corresponding radius, depending both on the approach and expansion. In particular, taking into consideration the most accurate method, that is the full expression in dynamical method, and the least accurate one, that is the parabolic approximation in thermodynamical method, an important deviation around 16% exists. In addition, it is notable that while the central values of the energy density of the thermodynamical method are similar, in the dynamical one, the full expression leads to slightly higher values. It is concluded that the effects of the crust-core interface on the minimum mass configuration are small but not negligible. Since the values of the central densities are even lower of the value of the saturation density $\rho_s \simeq 2.7 \times 10^{14} \text{ gr cm}^{-3}$, a final comment is appropriate. In this case, the structure of the core resembles a huge finite nuclei and thus, makes it an astronomical laboratory to check properties of low density nuclear matter. In view of the above statement, it will be of interest to study additional effects on the minimum mass configuration, including thermal and rotation effects, and moreover, to relate them with known properties of finite nuclei.

VI. CONCLUDING REMARKS

The values of the transition density and pressure are sensitive both on the order of the expansion of the total energy around the asymmetry parameter I , and also on

the employed method to locate the latter values. Moreover, we found that the lower the value of L the lower the deviation of the results. For higher values of L , the deviation becomes appreciable and must be taken into account in order to ensure the accuracy of applications. It is notable that using the full expression, the prediction of the transition density, in the case of the dynamical method, satisfies a kind of universal relation with the slope parameter which has been already suggested by Steiner *et al.* [53]. The corresponding predictions of the thermodynamical method are shifted to slightly higher values. These results confirm, once again, that dynamical method is more complete and consequently, more accurate compared to the thermodynamical one.

The latter results for n_t and P_t have been applied for the predictions of the bulk neutron star properties, which are related directly to the location of the crust-core transition. According to our findings, the effects are more pronounced on the crustal moment of inertia and the critical frequency related to r-mode instabilities. In contrast, the effects are less pronounced on the estimation of the tidal deformability but not negligible. Furthermore, in minimum mass configuration, while the effects are almost imperceptible for the minimum gravitational mass and the corresponding central energy density, a significant effect is presented in the corresponding radius.

Finally, we conclude that the dynamical method, in the framework of the full expression of the total energy, leads to more accurate predictions for the relevant neutron star properties. On the contrary, the most used thermodynamical method in the framework of the parabolic approximation, is responsible for the most roughly predictions.

ACKNOWLEDGMENTS

The authors would like to thank Prof. K. Kokkotas for his useful comments and insight and Mr. A. Kanakis-Pegios for the discussion and response about the tidal deformability issue.

[1] S.L. Shapiro and S.A. Teukolsky, *Black Holes, White Dwarfs, and Neutron Stars* (John Wiley and Sons, New York, 1983).

[2] N.K. Glendenning, *Compact Stars: Nuclear Physics, Particle Physics, and General Relativity*, (Springer, Berlin, 2000).

[3] P. Haensel, A.Y. Potekhin, and D. G. Yakovlev, *Neutron Stars 1: Equation of State and Structure* (Springer-Verlag, New York, 2007).

[4] C. Bertulani and J. Piekarewicz, *Neutron Star Crust*, (Nova, Space Science, Exploration and Policies, 2012).

[5] J.M. Lattimer and M. Prakash, *Phys. Rep.* **442**, 109 (2007).

[6] N. Paar, C.C. Moustakidis, T. Marketin, D. Vretenar, and G.A. Lalazissis, *Phys. Rev. C* **90**, 011304(R), (2014).

[7] M. Centelles, X. Roca-Maza, X. Vinas, M. Warda, *Phys. Rev. Lett.* **102**, 122502 (2009).

[8] C.J. Horowitz and J. Piekarewicz, *Phys. Rev. Lett.* **86**, 5647 (2001).

[9] G. Baym, H.A. Bethe and C.J. Pethick, *Nucl. Phys. A* **175**, 225 (1971).

[10] C.J. Pethick, D.G. Ravenhall, and C.P. Lorenz, *Nucl. Phys. A* **584**, 675 (1995).

[11] K. Oyamatsu and K. Iida, *Phys. Rev. C* **75**, 015801 (2007).

[12] C. Ducoin, Ph. Chomaz, and F. Gulminelli, *Nucl. Phys. A* **789**, 403 (2007).

- [13] J. Xu, L.W. Chen, B.A. Li, and H.R. Ma, *Astrophys. J.* **697**, 1549 (2009).
- [14] J.M. Lattimer and Y. Lim, *Astroph. J.* **771**, 51 (2013).
- [15] J. Fang, H. Pais, S. Pratapsi, and C. Providencia, *Phys. Rev. C* **95**, 062801(R) (2017).
- [16] M. Ferreira and C. Providencia, *Universe* **6**(11), 220 (2020).
- [17] L. Tsaloukidis, Ch. Margaritis, and Ch. C. Moustakidis, *Phys. Rev. C* **99**, 015803 (2019).
- [18] C. Gonzalez-Boquera, M. Centelles, X. Vinas, and A. Rios, *Phys. Rev. C* **96**, 065806 (2017).
- [19] S. Kubis, *Phys. Rev. C* **76**, 025801 (2007).
- [20] S. Kubis, *Phys. Rev. C* **70**, 065804 (2004).
- [21] Ch.C. Moustakidis, T. Niksic, G. A. Lalazissis, D. Vretenar, and P. Ring, *Phys. Rev. C* **81**, 065803 (2010).
- [22] Ch.C. Moustakidis, *Phys. Rev. C* **86**, 015801 (2012).
- [23] B.A. Li and M. Magno, *Phys. Rev. C* **102**, 045807 (2020).
- [24] J. Carriere, C.J. Horowitz, and J. Piekarewicz, *Astrophys. J.* **593**, 463 (2003).
- [25] H. Pais, A. Santos, L. Brito, and C. Providencia, *Phys. Rev. C* **82**, 025801 (2010).
- [26] H. Pais, A. Sulaksono, B. K. Agrawal, and C. Providencia, *Phys. Rev. C* **93**, 045802 (2016).
- [27] T. Carreau, F. Gulminelli, and J. Margueron, *Eur. Phys. J. A* **55**, 55 (2019).
- [28] Topical Issue on Nuclear Symmetry Energy, edited by B.A. Li, A. Ramos, G. Verde, and I. Vidana, *Eur. Phys. J. A* **50**, 2 (2014).
- [29] L. Perot, N. Chamel, and A. Sourie, *Phys. Rev. C* **101**, 015806 (2020).
- [30] J. Piekarewicz and F.J. Fattoyev, *Phys. Rev. C* **99**, 045802 (2019).
- [31] A. M. Kalaitzis, T. F. Motta and A. W. Thomas, *Int. J. Mond. Phys. E* **28**(09), 1950081 (2019).
- [32] F. Gittins, N. Andersson, and J.P. Pereira, *Phys. Rev. D* **101**, 103025 (2020).
- [33] B. Link, R.I. Epstein, and J.M. Lattimer, *Phys. Rev. Lett.* **83**, 3362 (1999).
- [34] F.J. Fattoyev and J. Piekarewicz, *Phys. Rev. C* **82**, 025810 (2010).
- [35] P.S. Koliogiannis and Ch.C. Moustakidis, *Phys. Rev. C* **101**, 015805 (2020).
- [36] N. Andersson and K.D. Kokkotas, *Int. J. Mod. Phys. D* **10**, 381 (2001).
- [37] J.L. Friedman and K.H. Lockitch, *Prog. Theor. Phys. Suppl.* **136**, 121 (1999).
- [38] N. Andersson, K. Kokkotas, and B.F. Schutz, *Astrophys. J.* **510**, 846 (1999).
- [39] Ch.C. Moustakidis, *Phys. Rev. C* **91**, 035804 (2015).
- [40] X. Zhou, A. Li, B.A. Li, R-mode Stability of GW190814's Secondary Component as a Supermassive and Superfast Pulsar (2021), arXiv: 2011.11934v2 [astro-ph].
- [41] B.P. Abbott *et al.*, *Phys. Rev. Lett.* **121**, 161101 (2018).
- [42] B.P. Abbott *et al.*, *Phys. Rev. X* **9**, 011001 (2019).
- [43] E.E. Flanagan and T. Hinderer, *Phys. Rev. D* **77**, 021502(R) (2008).
- [44] S. Postnikov, M. Prakash, and J.M. Lattimer, *Phys. Rev. D* **82**, 024016 (2010).
- [45] P. Haensel, J.L. Zdunik, and F. Douchin, *A&A* **385**, 301, (2002).
- [46] M. Colpi, S.L. Shapiro, and S.A. Teukolsky, *Astroph. J.* **339**, 318 (1989).
- [47] M. Prakash, I. Bombaci, M. Prakash, P.J. Ellis, J.M. Lattimer, and R. Knorren, *Phys. Rep.* **280**, 1 (1997).
- [48] Ch.C. Moustakidis and C.P. Panos, *Phys. Rev. C* **79**, 045806 (2009).
- [49] K. Hebeler, J.M. Lattimer, C.J. Pethick, and A. Schwenk, *Astroph. J.* **773**, 11 (2013).
- [50] E. Chabanat, P. Bonche, P. Haensel, J. Meyer, and R. Schaeffer, *Nucl. Phys. A* **627**, 710 (1997).
- [51] M. Farine, J.M. Pearson, and F. Tondeur, *Nucl. Phys. A* **615**, 135 (1997).
- [52] G. Baym, C. Pethik, and P. Sutherland, *Astrophys. J.* **170**, 299 (1971).
- [53] A.W. Steiner, S. Gandolfi, F.J. Fattoyev, and W.G. Newton, *Phys. Rev. C* **91**, 015804 (2015).
- [54] B. Link, R.I. Epstein, and J.M. Lattimer, *Phys. Rev. Lett.* **83**, 3362 (1999).
- [55] N. Andersson, K. Glampedakis, W.C.G. Ho, and C.M. Espinoza, *Phys. Rev. Lett.* **109**, 241103 (2012).
- [56] N. Chamel, *Phys. Rev. C* **85**, 035801 (2012).
- [57] B. Haskell, N. Degenaar, and W.C.G. Ho, *Mon. Not. R. Astron. Soc.* **424**, 93 (2012).